Available online at www.eccomasproceedia.org
Eccomas Proceedia COMPDYN (2025) 854- 866

ECCOMAS
Proceedia

COMPDYN 2025
10th ECCOMAS Thematic Conference on
Computational Methods in Structural Dynamics and Earthquake Engineering
M. Papadrakakis, M. Fragiadakis (eds.)
Rhodes Island, Greece, 15-18 June 2025

SEISMIC PERFORMANCE OF PINCHING-FREE TENSION-ONLY CBF EQUIPPED WITH METAL FOAM DAMPER

Annarosa Lettieri[1], Atsushi Sato[2], Massimo Latour[1], and Gianvittorio Rizzano[1]

[1] Department of Civil Engineering, University of Salerno, Fisciano, Italy
{alettieri,mlatour,g.rizzano}@unisa.it

[2] School of Engineering Nagoya Institute of Technology, Nagoya, Japan
sato.atsushi@nitech.ac.jp

Abstract

This work investigates the potentialities of using aluminium foam material (AFM) in an innovative aluminium foam damper (AFD) for Tension-Only CBFs (TO-CBFs) and X-braced CBFs with steel rods or tubes as bracings. The AFD device comprises aluminium foam layers, providing the structure with dissipative capacity and a wedge system to prevent a pinched global structural response. 1-storey TO-CBFs are designed according to Eurocode 8, and two configurations are considered: the conventional TO-CBFs and the innovative configuration equipped with AFDs denoted as Pinching-Free Tension-Only CBF (PF-CBF). The seismic performance of the structures is evaluated through Incremental Dynamic Analysis based on numerical models developed in OpenSees. The performances of the conventional and upgraded systems are compared, highlighting the effects resulting from the introduction of AFD into traditional systems. Moreover, additional local parameters in terms of displacements are monitored to quantify the seismic demand of the PF-CBFs and gain insights into the AFD design.

Keywords: Concentrically Braced Frames, Tension-only brace, Aluminium Foam Damper, Seismic Performance.

ISSN:2623-3347
Peer-review under responsibility of the organizing committee of COMPDYN 2025.
doi: 10.7712/120125.12696.24662

1 INTRODUCTION

Current codified seismic design procedures [1]-[3] promote structural damage to dissipate the seismic input energy and meet life safety requirements, often resulting in post-earthquake scenarios with severely damaged buildings, which affect community resilience [4],[5]. To overcome these drawbacks, earthquake engineering seeks innovative strategies to minimise seismic damage and socio-economic losses [6],[7].

Concentrically Braced Frames (CBFs) are widely used in high-rise buildings for their effectiveness in resisting lateral loads and limiting story drifts. CBFs resist seismic forces primarily through tension in diagonal bracings with a resisting mechanism vulnerable to brace buckling and fracture, leading to strength and stiffness deterioration [8]. Tension-Only CBFs (TO-CBFs) [9] have gained attention over the years for their cost-effectiveness and simplicity and for eliminating the risk of local buckling since very slender braces such as rods or tubesare used. TO-CBFs are widespread in North America and Japan, particularly in low- and mid-rise structures. At the same time, European regulations limit their use to low-rise buildings up to two stories [1]. Despite these advantages, both CBFs and TO-CBFs often exhibit poor energy dissipation capacity due to their pinched hysteretic response, and structural damage to conventional bracings remains unavoidable [10],[11].

Recent research studies have increasingly focused on developing innovative solutions to improve the hysteretic response of CBF structures. Some proposals include seismic dampers with slotted bolted connections [12], Added Damping and Stiffness (ADAS) steel dissipators [13], buckling restrained braces, and dissipative shear devices [14]. More recently, using innovative materials has been identified as a new topic to overcome existing challenges in developing seismic dampers for CBF structures [15]. In this context, Aluminium Foam Material (AFM) is an innovative material comprising heterogeneous cells of a gas phase within a metallic matrix characterised by enhanced plasticity, ultra-light structure, and significant energy dissipation capacity in compression compared to solid metals [16]. Currently, the applications of AFM are mainly focused on the automotive, military, and aerospace industries, while its use is limited in civil engineering. Among others, the use of sandwich panels in dry floors has been recently studied by Latour *et al*. [17] through experimental and numerical analyses on small-size panels glued through thin layers of bi-component epoxy resin. Moradi [18] investigated using AFM in thin-walled metal and foam-filled tubes to increase their ductility and buckling resistance.

This paper investigates using AFM in an Aluminium Foam Damper (AFD) to be employed in TO-CBFs and X-braced CBFs with steel rods or tubes as bracings (referred to as TO-CBF structures hereafter). The AFD includes a dissipative fuse consisting of AFM and a wedge system inspired by the solution proposed by Tamai and Takamatsu [19] to avoid a pinched global response. The work includes the AFD construction details, a tailored procedure for its design and the experimental characterisation of the AFM compressive behaviour. Successively, 1-storey TO-CBFs are designed according to Eurocode 8 [1] for two seismicity levels. Two configurations are considered for each case study: the conventional TO-CBFs and the innovative configuration equipped with AFDs denoted as Pinching-Free Tension-Only CBF (PF-CBF). Incremental Dynamic Analyses (IDA) [20] are carried out on simplified 2D FE models (i.e., plane frame model) developed in OpenSees [21] to assess the seismic performance of the structures. The seismic performances of the conventional and upgraded systems are compared, highlighting the effects resulting from the introduction of AFD into conventional systems.

2 ALUMINIUM FOAM DAMPER (AFD)

2.1 Constructional details and design procedure

Figure 1 shows the proposed AFD, conceptualised to be located within the bracing elements of TO-CBF structures with bracing elements realised with steel rods placed in S. Andrew's cross configuration (Figure 1(a)).

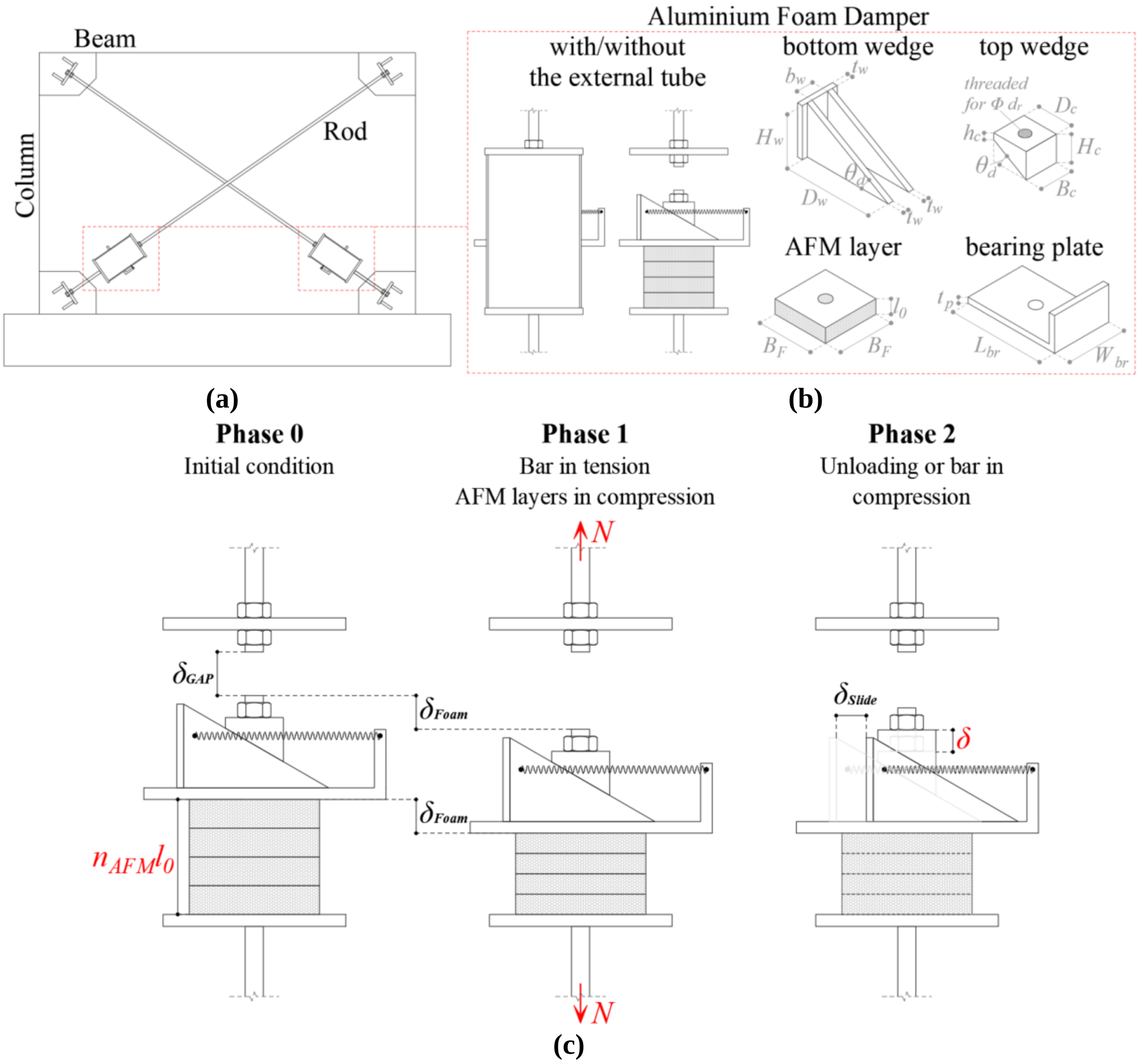

Figure 1: (a) AFD in a TO-CBF structure; AFD's (b) main components and (c) mechanism.

The AFD includes: 1) AFM cylindrical layers drilled to accommodate the rod diameter, which are expected to dissipate the input seismic energy accumulating compressive deformations; 2) a wedge system equipped with a double-spring system [19] to ensure the development of tensile forces in bracings while withstanding cyclic loadings. The wedge system consists of a top and a bottom component. The top element is connected to the rod through a threaded hole. The bottom part is a built-up element of three plates allowing the rod positioning. The inclined surfaces in contact are treated to obtain a friction coefficient greater than 0.6 [22],[23]; 3) a bearing plate to guarantee the transfer of stresses between the rods and the AFM layers as well as to allow the assembly of wedge and double-spring systems; 4) an external tube welded to squared endplates at the lower and upper ends, surrounding the AFM layers and the wedge components. The aforementioned main components of the AFD are depicted in Figure 1(b).

The dissipative mechanism of the AFD is schematically illustrated in Figure 1(c) through three distinct phases. In its initial condition (Phase 0), a clearance gap (i.e., δ_{GAP}) disconnects the rod within the device, allowing the bracing elements to slide for compressive deformations and, thus, prevent compression. Phase 1 displays the AFD working condition when the rod is subjected to tensile loading (i.e., N). At this stage, N is transmitted to the AFM layers through the wedge system and bearing plates, resulting in their compressive deformation (i.e., δ_{Foam}). It is noteworthy that, the top and bottom components do not slide relative to each other during the AFM compression. The firm contact is ensured by the friction developed at their interfaces in contact. Finally, in Phase 2, as the rod undergoes unloading or experiences compressive forces, the rod and the top wedge slide in compression, generating a gap with the bottom wedge(i.e., δ). The tension in the double-spring system allows the bottom wedge to slide horizontally (i.e., δ_{Slide}), maintaining continuous contact between the components and ensuring that the device remains operational for subsequent tensile cycles (Phase 1).

The design of the AFD is based on the structural analysis of the TO-CBF system at the design limit state (i.e., Ultimate Limit State, ULS) and requires as input values: the rod's diameter (i.e., d_r); the axial force acting on the rod at the ULS (i.e., N_{Ed}); the number of AFM layers (i.e., n_{AFM}); the overstrength that the AFM layers can provide to design non-dissipative components (i.e., $\gamma_{ov,AFM}$); the maximum expected compressive displacement in the AFM layers (i.e., $\delta_{Foam,max}$); the clearance δ_{GAP}. The design procedure involves the following key steps: 1) calculate the required net area of the AFM layers (i.e., A_f); 2) proportion the wedge system; 3) design the bearing plate; 4) design the external tube and the squared endplates at the lower and upper AFD ends. The AFM layers are designed as a dissipative component of the system, thus adopting N_{Ed} as design action. In contrast, the wedge system, bearing plate, external tube, and squared endplates, are properly over-strengthened to remain in the elastic range by considering $\gamma_{ov,AFM}*N_{Ed}$ as design force.

The required net area of the AFM layers (i.e., A_f) is calculated based on the yield strength of the foam material (i.e., $f_{y,AFM}$) as follows:

$$A_f \geq {N_{Ed}}/{f_{y,AFM}} \tag{1}$$

The AFM layers can be realised with cylinders with a circular or square cross-section and must include a concentric hole to accommodate d_r. Its dimension can be calculated as follows:

$$\phi_{ext} \geq \sqrt{\frac{4N_{Ed}}{\pi f_{y,AFM}} + {\Phi_{int}}^2} \tag{2}$$

$$B_F \geq \sqrt{\frac{N_{Ed}}{f_{y,AFM}} + \frac{\pi}{4}{\Phi_{int}}^2} \tag{3}$$

where Φ_{ext} is the external diameter of the AFM layers if a circular section is adopted; B_F is the dimension of the AFM layers if a square cross-section is adopted; Φ_{int} is the internal diameter of the concentric hole. Notably, to avoid contact between the rod and the AFM, a tolerance of 6.0 mm for the concentrical hole is suggested as a conservative value. For this reason, $\Phi_{int} \approx d_r + 6.0$ mm.

The dimensions of the wedge system depend on the rod diameter d_r. In particular, the configuration of the top wedge can be obtained as follows:

$$B_c = 2d_r \tag{4-a}$$

$$D_c = 3d_r \tag{4-b}$$

$$H_c = 3d_r \tan\theta_d + h_c \tag{4-c}$$

where B_c, D_c and H_c are, respectively, the top wedge's width, length, and height; θ_d is the angle of the inclined surface, equal to 30° in the present layout [22],[23]; h_c is equal to 20 mm to simplify the manufacturing process. Similarly, the bottom wedge's dimensions can be determined as follows:

$$b_w = d_r + 2.00\ mm \tag{5-a}$$

$$t_w = d_r/2 \tag{5-b}$$

$$H_w = 3d_r \tan\theta_d + \delta_{Foam,max} \tag{5-c}$$

$$D_w = H_w/\tan\theta_d \tag{5-d}$$

$$B_w = b_w + 2t_w \tag{5-d}$$

where b_w is the distance between the two plates with inclined surfaces, which has to guarantee no contact between the rod and the bottom wedge, and thus, a tolerance value of 2.00 mm is included; t_w is the thickness of the plates employed in the bottom wedge; B_w, D_w, and H_w, and are, respectively, the bottom wedge's width, length, and height.

The bearing plate's dimensions must guarantee the transmission of the axial forces into the AFM layers and accommodate the displacement of the bottom wedge (δ_{Slide}), and can be derived as follows:

$$L_{br} \geq 2(D_w - D_c + t_w) \tag{6-a}$$

$$W_{br} \geq max\{B_w; B_F; \phi_{ext}\} \tag{6-b}$$

where L_{br} and W_{br} are the length and width of the bearing plate, respectively. Moreover, the thickness of the bearing plate t_p is designed to resist the total force $\gamma_{ov,AFM}*N_{Ed}$ and to have sufficient stiffness, guaranteeing the full transmission of the forces to the AFM layers.

The external tube accommodates the wedge system, the bearing plate and the AFM layers and is designed to behave elastically. Based on its yield strength (i.e., $f_{y,c}$), the effective area (i.e., A_{ce}) can be obtained as follows:

$$A_{ce} \geq \gamma_{ov,AFM} N_{Ed} \big/ f_{y,c} \tag{7}$$

Circular and square sections can be employed for the external tube. It is noteworthy that, Eqn. (7) provide the minimum required value of A_{ce}. The external tube must surround the AFM layers and the wedge system. Moreover, a tube's opening must be included to allow the bearing plate placement. Specifically, the width of the external tube's opening (i.e., w_c) can be assumed to be equal to $w_c = W_{br} + 10$ mm, with a tolerance of 10 mm to ensure the correct positioning of the bearing plate.

2.2 Characterisation tests of AFM layers in compression

Four AFM layers are used in the investigated AFD layout, and this section presents the characterisation of their compressive behaviour. Figure 2 shows the experimental setup employed to evaluate the compressive behaviour of the AFM layers.

The tests were conducted at the StrEngTH Laboratory of the University of Salerno. Four samples of AFM with a nominal size of 90 mm x 90 mm x 42 mm were cut from larger panels with a nominal density of 510 kg/m^3 and assembled for testing in a four-layer configuration, as shown in Figure 2(a). Monotonic compressive tests were executed in transverse compression under displacement control. Besides, during the tests, unloading and subsequent reloading phases were introduced to evaluate the stiffness of the AFM. A Schenck Hydropuls S56 universal machine was used for the load application, and four Linear Variable Differential Transformers (LVDTs) were placed to monitor the axial displacement. The applied loads were measured using a loading cell.

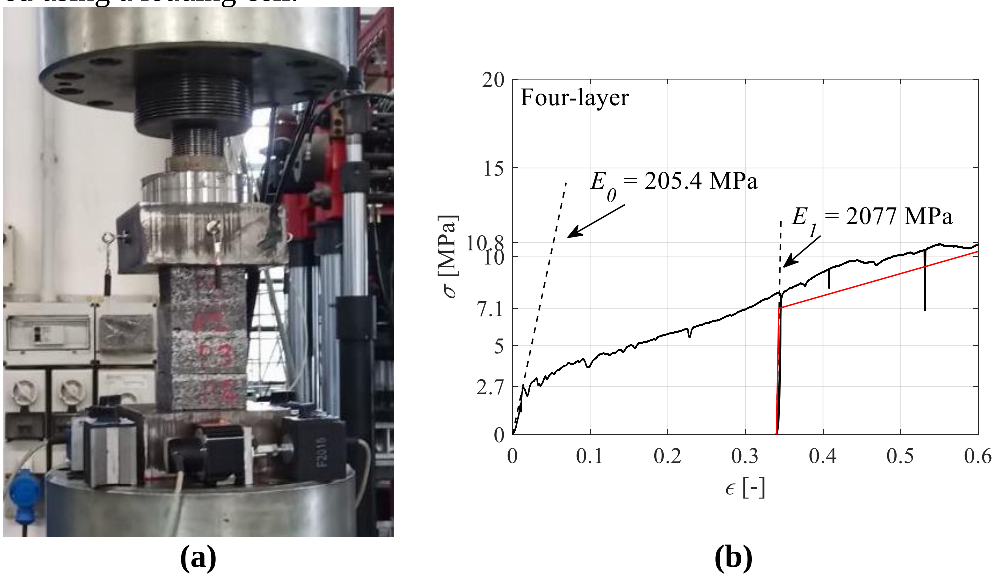

Figure 2: (a) Four-layer configurations of tested AFM sample and (b) experimental response regarding σ-ε.

The experimental response characterising the compressive behaviour of the AFM was registered in terms of stress-strain (i.e., σ-ε) and is reported in Figure 2(b). The results demonstrated the elastic-plastic AFM behaviour with an initial elastic response up to approximately 3% strain, characterised by an initial stiffness E_0, corresponding to the attainment of the yielding of the AFM (i.e., $f_{y,AFM}$). Subsequently, a strain-hardening phase is observed due to the densification of the AFM during the squashing, with a corresponding stiffness E_1.

A pre-squashing procedure was identified to increase the material's yield stress and allow the elastic modulus of the AFM (i.e., E_{AFM}) to reach the E_1 value. The procedure involves: 1) pre-loading of the AFM layers up to a strain level of about 30%. The stress corresponding to that strain level (i.e., 7.1 MPa) will represent the yield stress of the foam $f_{y,AFM}$ in its working condition; 2) unloading up to a strength value equal to zero.

Finally, the experimental results showed that the AFM can accommodate compressive deformations up to a total strain equal to 60%. Therefore, after the pre-squashing procedure, the four-layer AFM configuration can experience a total strain (i.e., ε_{max}) equal to 30%, corresponding to almost 50 mm (= 0.3 x 4 x 42 mm). The stress corresponding to that strain level (i.e., 10.8 MPa) represents the maximum stress the AFM layers can withstand (i.e., $f_{u,AFM}$). The overstrength value (i.e., $\gamma_{ov,AFM}$) provided by the AFM layers is equal to 1.5 (= 10.8 MPa / 7.1 MPa). Based on the experimental findings, a bi-linear analytical model describing the response of the four-layer AFM can be drawn (see Figure 2(b)).

3 CASE-STUDY STRUCTURES

3.1 Design of the case-study structures

Figure 3 shows the plan and elevation views of the case-study structures selected to investigate the seismic performance of TO-CBF structures equipped with the proposed AFD. Structures are 1-storey steel parking with a storey height of 3.50 m, while a span length of 5 m characterises all the bays. X-type TO-CBFs are set in the *x*- and *y*-directions, while the remaining part comprises gravity frames (with pinned beam-to-column connections and pinned column bases).

The study focuses on assessing the bracing configuration in the *x*-direction. Two configurations are analysed and compared for each case-study: the conventional TO-CBF structure and the PF-CBF, including the proposed AFD designed following the methodology presented in **Section 2.1**. In TO-CBF structures, bracings are realised with simple plates, while high-strength steel rods are used in the PF-CBF configurations. Steel S275 is employed for all structural elements (i.e., columns, beams, and braces).

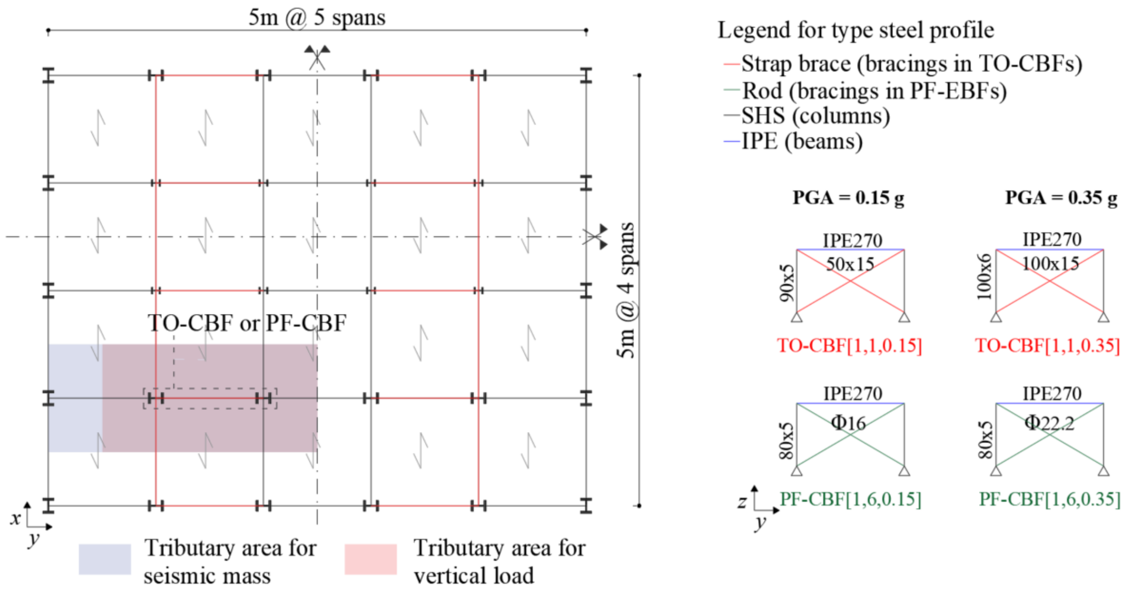

Figure 3: Plan and elevation views of the case-study structures.

All the structures have been proportioned according to Eurocode 8 [1], considering two seismicity levels. The design earthquake at the ULS is defined considering a Type-1 elastic response spectrum with a soil type C and a Peak Ground Acceleration (PGA) equal to 0.15 and 0.35g. The seismic action at the Collapse Limit State (CLS) is assumed to have an intensity equal to 150% of the ULS. Behaviour factors (i.e., q) equal to 1 and 6 are used for TO-CBFs and PF-CBF configurations, respectively. For PF-CBF, the q value is assumed to be similar to Buckling Strain Brace systems [1], reflecting the wide and stable hysteretic loops expected due to the inclusion of AFDs. No limitation about the non-dimensional slenderness (i.e., $\bar{\lambda}$) of the bracings has been included for both the TO-CBF and PF-CBF configurations. Notably, the bracings are intended to behave elastically in the PF-CBF configurations, and thus, the steel rods have been over-strengthened, considering an overstrength factor ($\gamma_{ov,AFM}$) equal to 1.5 according to the experimental characterisation (Figure 2(b)). The design results are reported in Figure 3. Table 1 lists all the case-study structures, indicating their fundamental periods of vibration T_1 and the spectral accelerations corresponding to the ULS (i.e., $S_a(T_1)_{ULS}$).

The AFDs have been proportioned for PF-CBF configurations, following the design procedure described in **Section 2.1**. The rods' diameters (d_r) and the design axial forces (N_{Ed}) have been derived based on the design structures at ULS. The four-layer AFM configuration has been chosen to be installed in the AFDs (n_{AFM} = 4). According to the experimental characterisation reported in **Section 2.2**, the AFM material's yield stress ($f_{y,AFM}$) and young modulus (E_{AFM}) are assumed to equal 7.1 and 2077 MPa, respectively. The AFM is designed to accommodate a maximum stroke ($\delta_{Foam,max}$) equal to 50 mm. Finally, the overstrength ($\gamma_{ov,AFM}$) value is assumed to be equal to 1.5. The main dimensions of the AFM layers' geometrical properties are indicated in Table 1.

Case-study	T_1 [sec]	$S_a(T_1)_{ULS}$ [g]	N_{Ed} [kN]	ϕ_{int} [mm]	ϕ_{ext} [mm]	$F_{y,AFM}$ [kN]	K_{AFM} [kN/m]
TO-CBF[1,1,0.15]	0.20	0.20	/	/	/	/	/
PF-CBF[1,6,0.15]	0.41	0.50	21	22	66	22	37521
TO-CBF[1,1,0.35]	0.14	1.00	/	/	/	/	/
PF-CBF[1,6,0.35]	0.29	1.20	63	28	112	65	114079

Table 1: Design results of the AFDs.

3.2 Case-study modelling

2D FE models (plane structural models) are developed in OpenSees [21] for all TO-CBFs and PF-CBFs. Figure 4(a) schematically shows the modelling strategy adopted. The '*section Aggregator*' function models the plastic shear capacity for columns, beams, and bracings. The '*Steel01*' material with 275 MPa yield strength and 0.2% post-yield stiffness ratio is employed for columns, bracings, and beams. Significant displacement effects of the frame elements are simulated through the *P-Δ* formulation (i.e., '*geomTransf PDelta*'). Moreover, the *P-Δ* effects due to the gravity frame are included by introducing a continuous leaning column pinned at the base.

The properties of the proposed AFD have been modelled by including zero-length elements placed in the axial direction of bracings. This modelling strategy is used for TO-CBF and PF-CBF configurations. Conversely, the material assigned to the zero-length element is different between the two models: the '*ElasticPPGap*' material is adopted for conventional TO-CBF, whereas the '*ElasticPP*' and '*Steel 01*' materials are combined in series to model the AFD behaviour in the PF-CBF. The AFM layers' behaviour has been included by specifying the yield strength (implemented as $F_{y,AFM} = f_{y,AFM} * A_f$) and the axial stiffness (implemented as $K_{AFM} = E_{AFM} * A_f / (n_{AFM} * l_0)$). The values of $F_{y,AFM}$ and K_{AFM} are reported in Table 1.

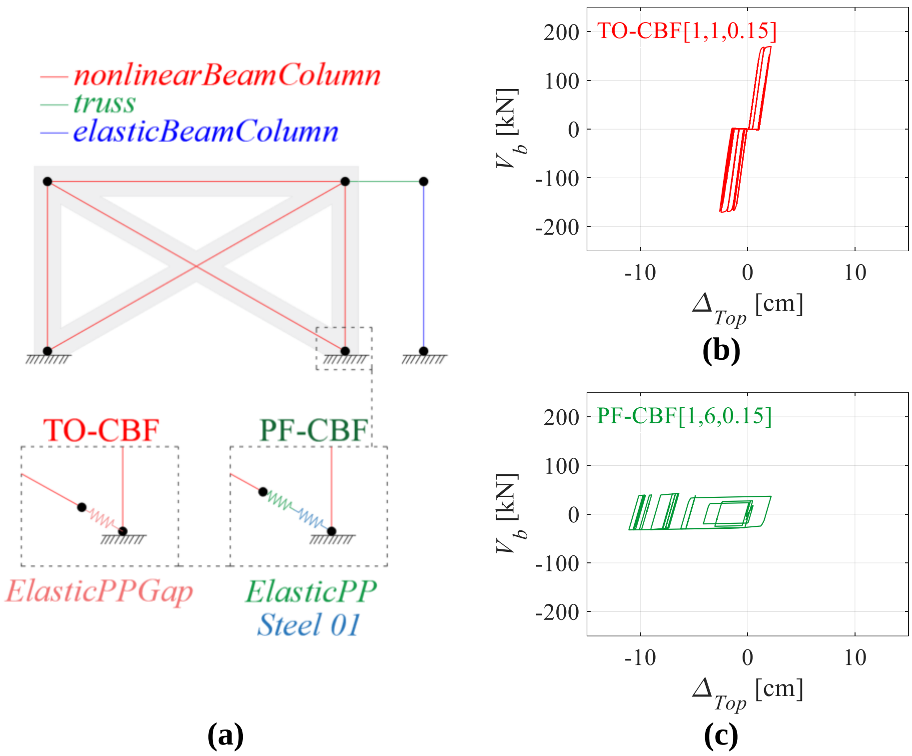

Figure 4: (a) OpenSees modelling; non-linear time hystory results in terms of V_b vs. Δ_{Top} for (b) TO-CBF[1,1,0.15] and (c) PF-CBF[1,6,0.15].

Non-linear time history analyses have been carried out for the case-study frame in both configurations (i.e., TO-CBF and PF-CBF) for one of the accelerograms of the set selected for PGA equal to 0.15g. Similar results are obtained for other case-study structures and accelerograms selected for PGA equal to 0.35g, but not reported for brevity. Figure 4(b) and (c) show the results in terms of shear base (i.e., V_b) vs. top displacement (i.e., Δ_{Top}) for TO-CBF[1,1,0.15] and PF-CBF[1,6,0.15], respectively. It is possible to observe that the response of the two frames aligns with expectations. The TO-CBF[1,1,0.15] exhibits a global behaviour characterised by significant pinching. In contrast, PF-CBF[1,6,0.15] shows a behaviour characterised by an upright and stable response, with higher dissipative capabilities. This is the result of the ratcheting system, which always allows the braces to activate immediately at the load reversal. Finally, in terms of resistance, the TO-CBF[1,1,0.15] shows a resistance about equal to six times that of the PF-CBF[1,6,0.15], as a consequence of different q factors adopted into their design.

4 INCREMENTAL DYNAMIC ANALYSES

IDAs [20] with 30 natural ground motions are used to evaluate the case-study structures' seismic performance. The records are selected using REXEL [24], considering a moment magnitude (i.e., M_w) ranging from 6 to 7, the epicentral distance $R \leqslant 30$ km, and spectrum compatibility in periods between 0.01 and 2 sec. To match the Eurocode 8 elastic response spectrum adopted for the design, the mean elastic spectrum of the records is kept considering superior and inferior tolerance limits equal to 30% and 25%, respectively.

The spectral acceleration corresponding to the fundamental period of vibration ($S_a(T_1)$) is assumed as the Intensity Measure (IM). Fixed steps of 0.1g are used to scale the accelerograms to cover the IM representing the main performance limit states until CLS. The seismic intensity levels are reported as dimensionless quantities, i.e., IM_N, defined by the ratio between $S_a(T_1)$

and $S_a(T_1)_{ULS}$. In this way, the IM_N intensities identifying the DLS, ULS and CLS limit states correspond to 0.5, 1.0 and 1.5, respectively.

Global Engineering Demand Parameters (EDPs) are monitored to investigate the seismic performance of the case-study structures. Maximum values of peak and residual interstorey drifts obtained among all stories of the structures (i.e., $\theta_{max\text{-}peak}$, $\theta_{max\text{-}res}$ respectively) are registered and synthesised by the 50%, 16%, and 84% fractiles among all ground motions. Additionally, for the PF-CBF configurations, the compressive accumulated deformation in AFD (i.e., δ_{Foam}) is recorded from the zero-length element as cumulated damage along the axial direction and reported as maximum among all the bracings within a structure.

Figure 5(a), and (b), respectively, compare the seismic performance of TO-CBF[1,1,0.15] vs. PF-CBF[1,6,0.15], TO-CBF[1,1,0.35] vs. PF-CBF[1,6,0.35], in terms of $\theta_{max\text{-}peak}$. The results generally indicate that structures in the TO-CBF configuration exhibit a contained peak response. In contrast, structures in the PF-CBF configuration show a more significant peak response due to using a higher behaviour factor, making the structures more flexible. It is important to note that PF-CBFs are designed for a behaviour factor q of 6 to account for the dissipative capabilities of the AFD device.

Figure 5(c), and (d), compare the seismic performance of TO-CBF[1,1,0.15] vs. PF-CBF[1,6,0.15], TO-CBF[1,1,0.35] vs. PF-CBF[1,6,0.35], in terms of $\theta_{max\text{-}res}$. As expected, the TO-CBF configurations undergo negligible permanent deformations. Conversely, the PF-CBF responses are characterised by consistent $\theta_{max\text{-}res}$ values. Although introducing the AFD devices provides structures with adequate dissipative capacity, it does not guarantee the reduction of residual deformations.

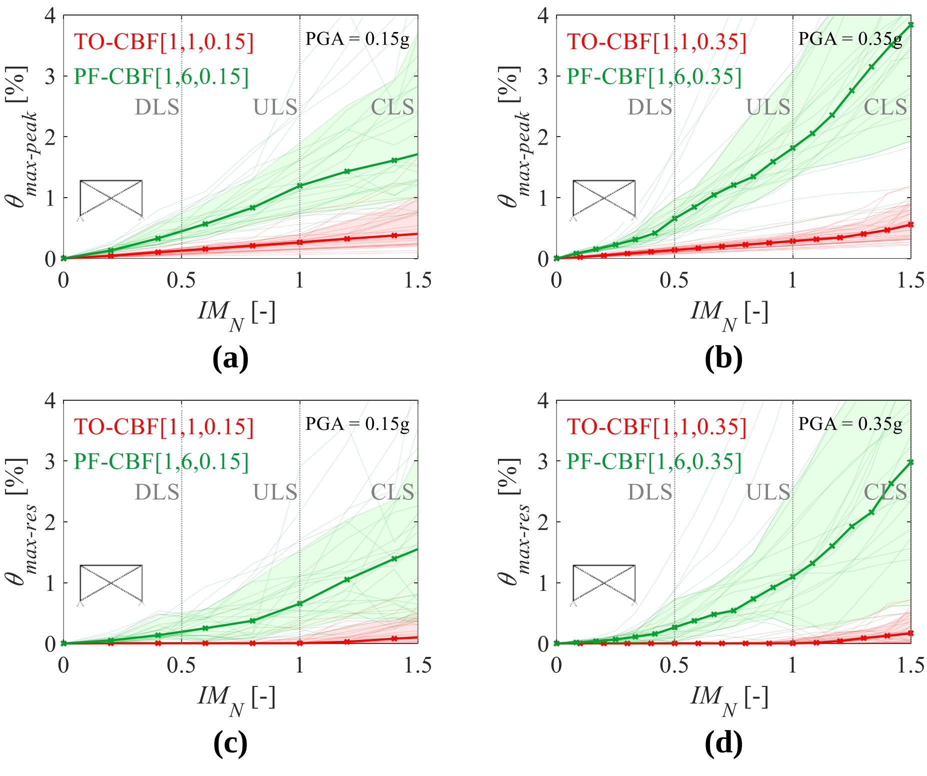

Figure 5: IDA results for TO-CBF[1,1,0.15] vs. PF[1,6,0.15] and TO-CBF[1,1,0.35] vs. PF[1,6,0.35] in terms of (a)-(b) $\theta_{max\text{-}peak}$ and (c)-(d) $\theta_{max\text{-}res}$.

Figure 6(a), and (b) report the IDA results in terms of δ_{Foam}, respectively for PF-CBF[1,6,0.15] and PF-CBF[1,6,0.35]. Additionally, the 50% fractile values at ULS are indicated in the figures to quantify the seismic demand values for AFDs at their design limit state. The results show that the 50% fractile of δ_{Foam} experiences values around 7 and 8 cm at ULS. Such values exceed the design value $\delta_{Foam,max}$ (i.e., 5 cm), potentially compromising the integrity of AFM layers employed in the AFDs and highlighting that four layers could be insufficient to accommodate the required seismic demand at the design limit state. Such results highlight the need to investigate an AFM configuration with six layers. Alternatively, the behaviour factor q used in the design shall be a smaller value, e.g., q = 4.0, and increase the design base share.

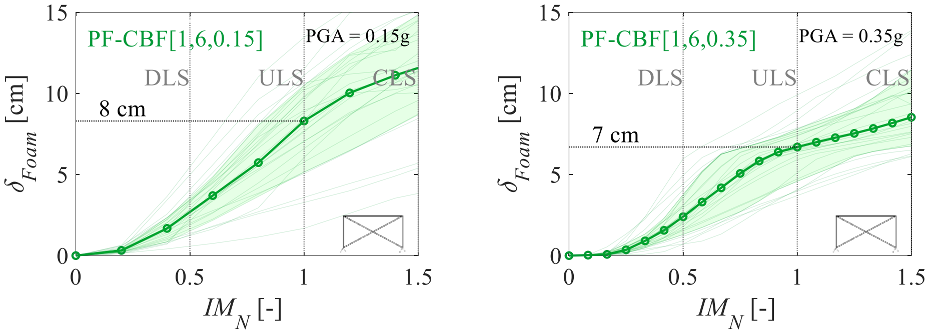

Figure 6: IDA results in terms of δ_{Foam} for (a) PF-CBF[1,6,0.15] and (b) PF-CBF[1,6,0.35].

5 CONCLUSIONS

This work investigates an Aluminium Foam Damper (AFD) for Tension-Only Concentrically Braced Frames (TO-CBF) and X-braced Concentrically Braced Frames (CBF) with bracings comprising very slender elements such as plates or rods. The AFD includes Aluminium Metal Foam (AFM) layers to provide structures with adequate dissipative capacity and a wedge system to avoid a pinched global response. The design procedure of the AFD is provided. The experimental response of the AFM layers is presented to define the analytical model representing its compressive behaviour. 1-storey X-braced CBFs steel frames with bracings comprising steel plates are adopted as case-studies to assess the main effects resulting from the introduction of AFD into conventional systems. Structures are designed according to Eurocode 8, and two configurations are considered: the conventional TO-CBFs and the innovative configuration equipped with AFDs denoted as Pinching-Free Tension-Only CBF (PF-CBF). Simplified 2D FE models have been developed in OpenSees to assess the seismic performance of the case-studies. Incremental Dynamic Analyses (IDA) are performed with 30 ground motion records, assessing global and local engineering demand parameters while accounting for the record-to-record variability. The following main outcomes can be drawn: (1) the experimental tests characterising the compressive behaviour of the AFM showed the possibility of representing its analytical behaviour through a bi-linear model similar to steel; (2) the OpenSees results showed that the introduction of the AFD in TO-CBF allows for improvement of their dissipative capacity and avoiding a hysteretic response characterised by a pinching behaviour; (3) structures in their PF-CBF configuration can experience high peak and residual deformations, compared to TO-CBFs, suggesting the need to investigate the adoption of lower design behaviour factors.

REFERENCES

[1] CEN (European Committee for Standardization). 2004. Eurocode 8: Design of structures for earthquake resistance – Part 1: General rules, seismic actions and rules for buildings. EN 1998-1, Brussel, Belgium: CEN.

[2] ASCE/SEI 7–22, Minimum Design Loads and Associated Criteria for Buildings and Other Structures, American Society of Civil Engineers, 2 022. https://doi.org/10.1061/9780784415788.

[3] BCJ, The Building Standard Law of Japan, 2016.

[4] F. Freddi, V. Novelli, R. Gentile, E. Veliu, A. Andonov, S. Andreev, F. Greco, E. Zhuleku, Observations from the 26th November 2019 Albania earthquake: the earthquake engineering field investigation team (EEFIT) mission. *Bulletin of Earthquake Engineering*, **19**, 2013-2044, 2021. https://doi.org/10.1007/s10518-021-01062-8.

[5] C. Clifton, M. Bruneau, G. MacRae, R. Leon, A. Fussell, Steel structures damage from the Christchurch earthquake series of 2010 and 2011. *Bulletin of the New Zealand Society for Earthquake Engineering*, **44**(4), 297-318, 2011. https://doi.org/10.5459/bnzsee.44.4.297-318.

[6] F. Freddi, C. Galasso, G. Cremen, A. Dall'Asta, L. Di Sarno, A. Giaralis, L.F. Gutiérrez-Urzúa, C. Málaga-Chuquitaype, S. Mitoulis, C. Petrone, A. Sextos, L. Sousa, K. Tarbali, E. Tubaldi, J. Wardman, G. Woo, Innovations in Earthquake Risk Reduction for Resilience: Recent Advances and Challenges. *International Journal of Disaster Risk Reduction*, 60: 102267, 2021. https://doi.org/10.1016/j.ijdrr.2021.102267.

[7] A. Lettieri, E. Elettore, L. Pieroni, F. Freddi, M. Latour, G. Rizzano, Parametric analysis of steel MRFs with self-centring column bases. *Steel Construction*, 2022 https://doi.org/10.1002/stco.202100050

[8] C.W. Roeder, E.J. Lumpkin, D.E. Lehman, Seismic performance assessment of concentrically braced steel frames. *Earthquake spectra*, **28**(2), 709-727, 2012. https://doi.org/10.1193/1.4000006.

[9] FEMA P-695 (2009) Quantification of building seismic performance factors. Federal Emergency Management Agency, Washington, DC.

[10] R. Tremblay, A. Filiatrault, Seismic impact loading in inelastic tension - only concentrically braced steel frames: myth or reality?. *Earthquake engineering & structural dynamics*, **25**(12), 1373-1389, 1996. https://doi.org/10.1002/(SICI)1096-9845(199612)25:12%3C1373::AID-EQE615%3E3.0.CO;2-Y.

[11] A. Filiatrault, R. Tremblay, Design of tension-only concentrically braced steel frames for seismic induced impact loading. *Engineering Structures*, 20(12), 1087-1096, 1998. https://doi.org/10.1016/S0141-0296(97)00205-8.

[12] T.F. Fitzgerald, T. Anagnos, M. Goodson, T. Zsutty, Slotted bolted connections in aseismic design for concentrically braced connections. *Earthquake spectra*, 5(2), 383-391, 1989. https://doi.org/10.1193/1.1585528.

[13] C. Xia, R.D. Hanson, Influence of ADAS element parameters on building seismic response. *Journal of Structural Engineering*, 118(7), 1903-1918, 1992. https://doi.org/10.1061/(ASCE)0733-9445(1992)118:7(1903).

[14] G. Della Corte, M. D'Aniello, R. Landolfo, F. Mazzolani, Review of steel buckling - restrained braces. *Steel construction*, 4(2), 85-93, 2011. https://doi.org/10.1002/stco.201110012.

[15] C. Fang, W. Wang, C. Qiu, S. Hu, G.A. MacRae, M.R. Eatherton, Seismic resilient steel structures: A review of research, practice, challenges and opportunities. *Journal of Constructional Steel Research*, 191, 107172, 2022. https://doi.org/10.1002/eqe.3733.

[16] B.H. Smith, S. Szyniszewski, J.F. Hajjar, B.W. Schafer, S.R. Arwade, Steel foam for structures: A review of applications, manufacturing and material properties. *Journal of Constructional Steel Research*, 71, 1-10, 2012. https://doi.org/10.1016/j.jcsr.2011.10.028.

[17] M. Latour, A. Sato, M. D'Aniello, R. Landolfo, G. Rizzano, Flexural response of metallurgically bonded steel-aluminium foam-steel panels and composite beams. *Engineering Structures*, 322, 119114, 2025. https://doi.org/10.1016/j.engstruct.2024.119114.

[18] M. Moradi, *Structural applications of metal foams considering material and geometrical uncertainty*. University of Massachusetts Amherst, 2011.

[19] H. Tamai, T. Takamatsu, Cyclic loading tests on a non-compression brace considering performance-based seismic design. *Journal of Constructional Steel Research*, 61(9), 1301-1317, 2005. https://doi.org/10.1016/j.jcsr.2005.01.009.

[20] D. Vamvatsikos, C.A. Cornell, Incremental Dynamic Analysis. *Earthquake Engineering Structural Dynamics*, 31(3), 491-514, 2002.

[21] S. Mazzoni, F. McKenna, M.H. Scott, G.L. Fenves, *Computer Program OpenSees: Open System for Earthquake Engineering Simulation*, Pacific Earthquake Engineering Research Center (PEER). University of California, Berkeley, California, 2009. Available at: http://opensees.berkeley.edu.

[22] A. de la Peña, A. Sato, M. Latour, G. Rizzano, Conceptual design of anti-seismic devices with metal foam core for CBFs. *Procedia Structural Integrity*, 44, 2144-2151, 2023. https://doi.org/10.1016/j.prostr.2023.01.274.

[23] A. Sato, M. Latour, G. Rizzano, Development of pinching‐free tension‐only CBFs based on the application of metal foam dampers. *ce/papers*, 6(3-4), 2381-2387, 2023. https://doi.org/10.1002/cepa.2711.

[24] I. Iervolino, C. Galasso, E. Cosenza, REXEL: Computer aided record selection for code-based seismic structural analysis. *Bulletin of Earthquake Engineering*, 8, 339-362, 2010.